Signatures for Viral Infection and Inflammation in the Proximal Olfactory System in Familial Alzheimer's Disease

Andrew N. Bubak[1,‡], Laetitia Merle[2,3,‡], Christy S. Niemeyer[1], B. Dnate' Baxter[2,3], Arianna Gentile Polese[2,3], Vijay Ramakrishnan[4], Johana Gomez[5], Lucia Madrigal[5], Andres Villegas-Lanau[5], Francisco Lopera[5], Wendy Macklin[1,2], Seth Frietze[6], Maria A. Nagel[1,7#], and Diego Restrepo[1,2, #,*]

[1]Department of Neurology, University of Colorado Anschutz Medical Campus, Aurora, CO 80045, USA

[2]Neuroscience Graduate Program, University of Colorado Anschutz Medical Campus, Aurora, CO 80045, USA

[3]Department of Cell and Developmental Biology, University of Colorado Anschutz Medical Campus, Aurora, CO 80045, USA

[4]Department of Otolaryngology-Head and Neck Surgery, Indiana University School of Medicine, Indianapolis, IN 46202, USA

[5]Neuroscience Research Group, University of Antioquia, Medellín, Colombia

[6]Department of Medical Laboratory Sciences, University of Vermont, Burlington, VT

[7]Department of Opthalmology, University of Colorado Anschutz Medical Campus, Aurora, CO 80045, USA

[‡]Co-first authors

[#]Senior authors

[*]Corresponding author: Diego Restrepo, diego.restrepo@cuanschutz.edu

Acknowledgements: This study was funded by NIA Administrative supplements to NIDCD DC014253 and DC000566. TempO-Seq and nanoString graphics were created with BioRender.com.

Abstract

Alzheimer's disease (AD) is characterized by loss of smell and olfactory system pathology that subsequently leads to dementia. Understanding these early processes can identify therapeutic targets to slow AD progression. Thus, we analyzed differential gene and protein expression in the olfactory bulb (OB) and olfactory tract (OT) of familial AD (FAD) individuals carrying the autosomal dominant presenilin 1 E280A paisa mutation and age-matched controls. In FAD samples, we find human transcriptome signatures for viral infection in OB and for inflammation in OT that carries information via entorhinal cortex from the OB to hippocampus, a brain region essential for learning and memory. Interestingly, spatial proteomic changes consistent with a demyelination response in the OT of FAD individuals were seen, implying dysfunction of communication between the OB and hippocampus. These findings raise the possibility that viral infection and associated inflammation/demyelination of the olfactory system may disrupt downstream hippocampal function, accelerating FAD pathogenesis.

45 A critical barrier in treating Alzheimer's disease (AD) is the years- to decades-long lag
46 from disease onset to the diagnosis of dementia, when reversal of brain pathology and
47 recovery of neurons may, at best, slow cognitive decline. Thus, it is essential to identify
48 contributory pathological processes in early disease to prevent progression to dementia,
49 disability and death. An early process in AD, prior to clinical dementia, is a deficit in the
50 sense of smell[1] accompanied by β-amyloid (Aβ) deposition in the OB that receives
51 olfactory input from olfactory sensory neurons in the olfactory epithelium[2,3].
52 Understanding the cellular basis for this loss of smell is important because of the
53 potential use of cellular changes in early diagnosis, and because olfactory dysfunction
54 may play a role in the etiology of AD. However, little is known about changes in the
55 cellular processes of proximal brain areas of the olfactory system, the OB and the OT
56 that carries information to downstream brain processing areas including entorhinal
57 cortex and the hippocampus, a brain region that plays a key role in learning and
58 memory. Here, we use TempO-Seq, a novel technique optimized to perform reliable
59 transcriptome analysis from formalin-fixed, paraffin-embedded human tissue samples[4],
60 to characterize differences in the transcriptome of the OB and OT in familial AD (FAD)
61 individuals versus age-matched controls. We study the human transcriptome in
62 Colombian presenilin 1 E280A mutation carriers that develop mild cognitive
63 impairment (MCI) and dementia at the respective median ages of 44 (95% CI, 43–45)
64 and 49 (95% CI, 49–50) years old[5].
65
66 Prior to transcriptome analysis, we analyzed the tissue for morphology and composition.
67 Figure 1 A-C shows immunohistochemistry analysis of the human OT from FAD subjects
68 and age-matched controls (Supplementary Table 1). Staining for the myelin marker

69 proteolipid protein (PLP) showed that the OT included high and low myelination areas
70 (Fig. 1A, see Supplementary Table 2 for antibodies used). We did not find a difference
71 between FAD and controls in the area occupied by the high/low myelinated regions in
72 the OT (Fig. 1A). As expected, we found increased immunostaining for Aβ in the OT of
73 FAD subjects compared to controls (Fig. 1B). In addition, as expected for
74 neuroinflammation in AD, and consistent with prior studies in spontaneous AD[6], we
75 found increased immunostaining for the microglia/macrophage markers Iba1 and CD68
76 in FAD OT compared to control (Fig. 1C). Finally, we found increased association
77 between CD68 and Iba1 and between Aβ and microglia whose association has been
78 proposed to constitute a barrier with profound impact on Aβ plaque composition and
79 toxicity[7] (Supplementary Figure 1).
80
81 We then performed TempO-seq targeted RNA sequencing analysis of the OT and OB
82 from 6 FAD individuals who did not die of virus infection and 4 age-matched controls
83 (Supplementary Table 1). Compared to controls, we found 1,319 differentially expressed
84 genes (DEGs) in FAD OT and 2,775 significantly DEGs in FAD OB. Volcano plots in
85 Figs. 1Di (OT) and 1Fi (OB) show that the majority of DEGs displayed increased
86 expression in FADs (also see Supplementary Tables 3 and 4). When we deconvolved the
87 DEGs to estimate glial surrogate proportions, we found that microglia were higher in
88 FAD samples (Fig. 1E), consistent with the immunohistochemistry results for Iba1 and
89 CD68 (Fig. 1C). Interestingly, in the deconvolution, we found decreased surrogate
90 proportion for oligodendrocytes in FAD (Fig. 1E). Further, human gene-set enrichment
91 analyses in the FAD OB showed multiple upregulated transcriptional pathways
92 associated with viral infection, including “Viral infection”, “Infection of cells”, and

93 “Replication of virus” (Fig. 1Fii), whereas the OT of FAD individuals represented an
94 upregulation of immune response signatures that included “IL-6 signaling”, “IL-8
95 signaling”, “Natural killer cell signaling”, “Jak/Stat signaling”, “Neuroinflammation
96 signaling”, and “Production of nitric oxide and reactive oxygen species in macrophages,”
97 as well as the expected “Amyloid processing” pathway (Fig. 1 Dii). Observed genes in
98 each pathway are shown in Supplementary Table 5.
99
100 We performed complementary nanoString spatial proteomics analysis[8] for 88
101 proteins including markers for AD and immune responses (Supplementary Table 6) in
102 tissue regions discriminated based on fluorescent markers for myelin basic protein, Aβ,
103 Iba1 and nuclear staining (see Methods and Supplementary Table 7). The four tissue
104 regions were high myelination and low myelination OT, and glomerular layer/external
105 plexiform layer and granule cell layer in the OB (Fig. 2A, Supplementary Figure 2).
106 nanoString proteomics showed spatial protein specificity involved in immune and AD
107 responses in the OT and to a lesser extent in the OB (Fig. 2B). Interestingly, both the
108 immune and AD marker responses differ between regions. For example the increase in
109 AD markers in FAD was most marked in the low myelinated OT, and there were
110 increases in immune markers in both low and high myelinated OT, but they were
111 heterogeneous between these two brain regions and much lower in the OB indicating
112 that the immune response differs between brain areas in the proximal olfactory system
113 (Fig. 2B). Strikingly, principal component analysis (PCA) of the spatial proteomics
114 results shows orthogonal localization of FAD versus control proteomics regardless of the
115 tissue region (Fig. 2C). Furthermore, there were marked differences in protein
116 expression between brain regions within the experimental groups (FAD and control,

117 Figs. 2D, Supplementary Figure 3). Interestingly, within the FAD cohort a large group of
118 proteins involved in response to demyelination were expressed at high levels in high
119 myelination OT compared to all other regions (group A in Fig. 2Dii) and a group of AD
120 markers was expressed at high levels in the low myelination OT (group B in Fig. 2Dii)
121 (Supplementary Note 1).
122
123 Our findings reveal a transcriptomic signature for viral infection of the OB coupled with
124 inflammation and problems with myelination in the OT in FAD, confirmed by proteomic
125 analysis. While our studies only identified human transcripts/proteins and were not
126 designed to identify specific viruses, the most likely viruses contributing to olfactory
127 system infection and potential CNS dysfunction are the 2 neurotropic
128 alphaherpesviruses, herpes simplex virus type-1 (HSV-1) and varicella zoster virus
129 (VZV). HSV-1 and VZV are strong candidates for being initiators or accelerators of AD
130 because they increase dementia risk and elicit the same pathological characteristics of
131 AD, including amyloid accumulation, neuroinflammation, neurodegeneration, and
132 cognitive impairment[9-11]. Furthermore, this family of alphaherpesviruses is latent in
133 trigeminal ganglia which innervates the OE/OB[12], providing a direct internal route of
134 virus entry during reactivation. Our studies find that even in patients predisposed to AD
135 due to a genetic mutation of PS1 there is evidence of viral infection in the OB suggesting
136 that viral infection and inflammatory response in the OT are part of the etiology of the
137 disease. Taken together with a parallel body of literature indicating that early AD is
138 characterized by smell loss[1], amyloid deposition in the olfactory epithelium (OE), and
139 olfactory sensory neuron (OSN) dysfunction[3] our study raises the possibility that viral
140 infection of the OB/OT accelerates AD. Because sniff-induced beta and theta-coupled

141 gamma oscillations generated in the OB are directionally coupled to the hippocampus[13-
142 16], smell loss would result in decreased hippocampal gamma oscillations that have been
143 postulated to lead to neurodegeneration and cognitive decline.[17-19] These studies suggest
144 that alphaherpesvirus disruption of olfactory pathways can accelerate AD cognitive
145 decline (Supplementary Figure 4).
146

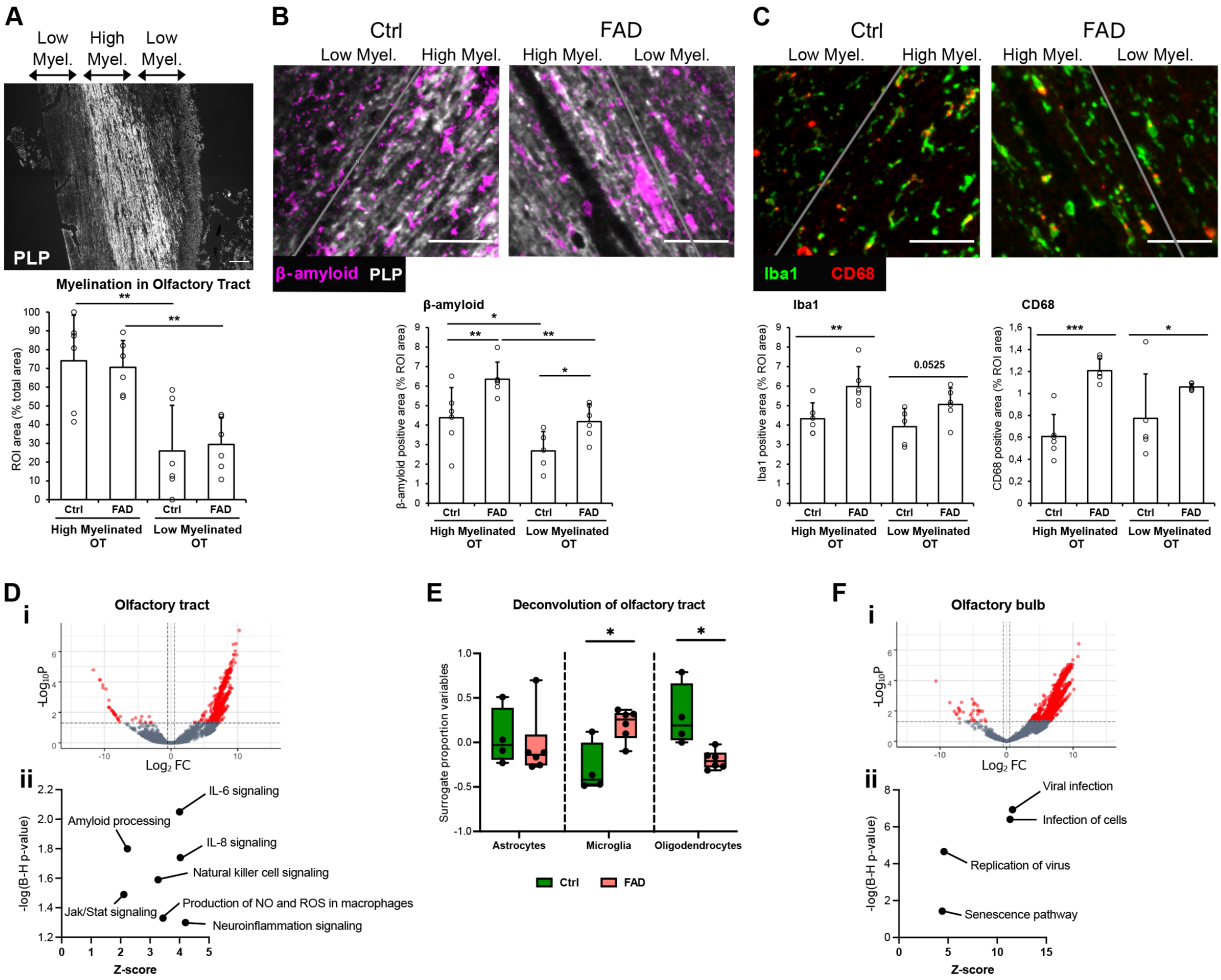

Figure 1. Immunohistochemistry of the human OT and TempO-Seq transcriptome analysis of the OB and OT. A-C. IHC of the human OT for 6 control and 6 FAD subjects. A. PLP stain was used to delimitate the high and low myelinated regions in OT. The bar graph represents the mean surface of high and low myelinated regions per individual, expressed as a percentage of the total area analyzed. An ANOVA yields no significant difference for the genotype F=0.1, 1 d.f., p>0.05 and a significant difference between high and low myelination areas F=26.84, 1 d.f., p<0.001. B. Representative images and quantification of Aβ in the OT from 6 Ctrl and 6 FAD patients. Aβ positive surface is increased in FAD patients compared to control, in both

158 the high and low myelinated OT. Within the FAD group, the accumulation of Aβ is
159 higher in the high myelinated than the low myelinated OT. ANOVA yields a significant
160 difference for the genotype $F=13.94$, 1 d.f., $p<0.01$ and a significant difference between
161 high and low myelination areas $F=17.22$, 1 d.f., $p<0.001$. C. Quantification of
162 microglia/macrophage markers Iba1 and CD68, showing increased neuroinflammation
163 in the high myelinated OT. ANOVA for Iba1 and CD68 yields a significant difference for
164 genotype (Iba1, $F=13.54$, 1 d.f., $p<0.01$, CD68, $F=23.24$, 1 d.f., $p<0.001$). D and F.
165 Volcano plot for TempO-Seq (top) and insight pathway analysis of transcriptional
166 differences (bottom) for the OT (D) and OB (F). E. Deconvolution of the transcriptional
167 differences for the OT. Asterisks are significant p values for post-hoc Fisher's least
168 significant difference.
169

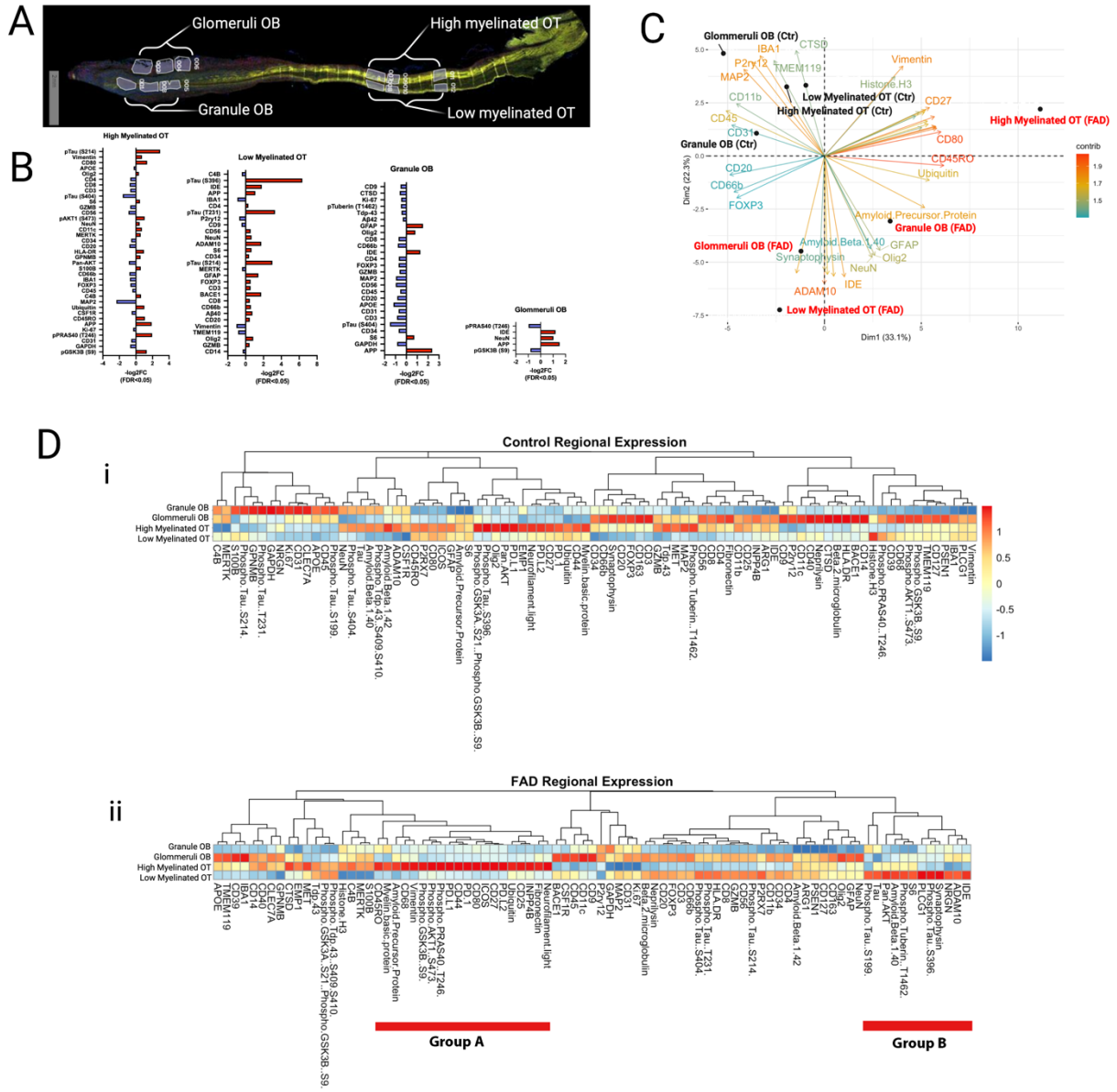

Figure 2. nanoString proteomic analysis of OB and OT expression of markers for AD and immunity. A. Representative tissue section stained for myelin basic protein (MBP) showing the regions that were used for protein quantification. In the OB "Glomeruli OB" included the glomerular layer (GL) and the external plexiform layer (EPL), "Granule OB" included the granule cell layer and the accessory olfactory nucleus (AON). In the OT the high and low myelinated areas were determined by high and low MBP staining. B. Log 2 fold change for the levels of protein expression in the

178 different tissue regions. Red denotes higher expression in FAD. Only the proteins whose
179 levels are significantly different between genotypes are shown. C. Principal component
180 analysis of the protein levels of expression. D. Pseudocolor plots comparing between
181 regions the levels of expression for all proteins. Proteins are segregated by Euclidean
182 distance calculated by the total normalized reads for each protein between tissue regions
183 or samples. i. Control tissue. ii. FAD. Group A are adjacent proteins that display higher
184 levels in high myelinated OT and group B are adjacent proteins that display higher levels
185 in low myelinated OT.
186

187 **References**

188 1. Murphy, C. Olfactory and other sensory impairments in Alzheimer disease. *Nat Rev Neurol*
189 **15**, 11-24 (2019).

190 2. Attems, J., Walker, L. & Jellinger, K.A. Olfactory bulb involvement in neurodegenerative
191 diseases. *Acta Neuropathologica* **127**, 459-475 (2014).

192 3. Dibattista, M., Pifferi, S., Menini, A. & Reisert, J. Alzheimer's Disease: What Can We
193 Learn From the Peripheral Olfactory System? *Frontiers in Neuroscience* **14**, 440 (2020).

194 4. Trejo, C.L.*, et al.* Extraction-free whole transcriptome gene expression analysis of FFPE
195 sections and histology-directed subareas of tissue. *PLoS One* **14**, e0212031 (2019).

196 5. Acosta-Baena, N.*, et al.* Pre-dementia clinical stages in presenilin 1 E280A familial early-
197 onset Alzheimer's disease: a retrospective cohort study. *The Lancet Neurology* **10**, 213-220
198 (2011).

199 6. Kohl, Z.*, et al.* Distinct Pattern of Microgliosis in the Olfactory Bulb of Neurodegenerative
200 Proteinopathies. *Neural Plasticity* **2017**, 3851262 (2017).

201 7. Grutzendler, J., Yang, G., Pan, F., Parkhurst, C.N. & Gan, W.B. Transcranial two-photon
202 imaging of the living mouse brain. *Cold Spring Harb Protoc* **2011**(2011).

203 8. Merritt, C.R.*, et al.* Multiplex digital spatial profiling of proteins and RNA in fixed tissue.
204 *Nature Biotechnology* **38**, 586-599 (2020).

205 9. Eimer, W.A.*, et al.* Alzheimer's Disease-Associated beta-Amyloid Is Rapidly Seeded by
206 Herpesviridae to Protect against Brain Infection. *Neuron* **99**, 56-63 e53 (2018).

207 10. Readhead, B.*, et al.* Multiscale Analysis of Independent Alzheimer's Cohorts Finds
208 Disruption of Molecular, Genetic, and Clinical Networks by Human Herpesvirus. *Neuron*
209 **99**, 64-82 e67 (2018).

210 11. Itzhaki, R.F. & Lathe, R. Herpes Viruses and Senile Dementia: First Population Evidence
211 for a Causal Link. *J Alzheimers Dis* **64**, 363-366 (2018).
212 12. Schaefer, M.L., Bottger, B., Silver, W.L. & Finger, T.E. Trigeminal collaterals in the nasal
213 epithelium and olfactory bulb: a potential route for direct modulation of olfactory
214 information by trigeminal stimuli. *J Comp Neurol* **444**, 221-226 (2002).
215 13. Gourevitch, B., Kay, L.M. & Martin, C. Directional coupling from the olfactory bulb to
216 the hippocampus during a go/no-go odor discrimination task. *J Neurophysiol* **103**, 2633-
217 2641 (2010).
218 14. Martin, C., Beshel, J. & Kay, L.M. An olfacto-hippocampal network is dynamically
219 involved in odor-discrimination learning. *J.Neurophysiol.* **98**, 2196-2205 (2007).
220 15. Pena, R.R.*, et al.* Home-cage odors spatial cues elicit theta phase/gamma amplitude
221 coupling between olfactory bulb and dorsal hippocampus. *Neuroscience* **363**, 97-106
222 (2017).
223 16. Nguyen Chi, V.*, et al.* Hippocampal Respiration-Driven Rhythm Distinct from Theta
224 Oscillations in Awake Mice. *J Neurosci* **36**, 162-177 (2016).
225 17. Iaccarino, H.F.*, et al.* Gamma frequency entrainment attenuates amyloid load and modifies
226 microglia. *Nature* **540**, 230-235 (2016).
227 18. Gillespie, Anna K.*, et al.* Apolipoprotein E4 Causes Age-Dependent Disruption of Slow
228 Gamma Oscillations during Hippocampal Sharp-Wave Ripples. *Neuron* **90**, 740-751
229 (2016).
230 19. Salimi, M.*, et al.* Disrupted connectivity in the olfactory bulb-entorhinal cortex-dorsal
231 hippocampus circuit is associated with recognition memory deficit in Alzheimer's disease
232 model. *Scientific Reports* **12**, 4394 (2022).

233 **Methods**

234

235 Standard protocol approvals, registrations, and participant consent.

236 We study the transcriptome in the OB and OT in Colombian presenilin 1 (PSEN1)
237 E280A mutation carriers[1] and age-matched controls. The institutional review board
238 committee at the University of Antioquia (Colombia) approved tissue collection for this
239 study. Participants provided written informed consent before participating. A total of 6
240 members from Colombian families with the *PSEN1* E280A mutation and 6 age-matched
241 controls participated in the study. The demographic data for all participants included in
242 this report are detailed in Supplementary Table 1 (a breakdown by study is provided in
243 eTable1). Mutation carriers have a previously documented median expected age at onset
244 of MCI at 44 years of age (95% confidence interval [CI] = 43–45 years) and dementia
245 due to AD at 49 years of age (95% CI = 49–50 years).[2] Eligible individuals were
246 screened for neurological and psychiatric disorders, and they did not die of viral
247 pneumonia. Clinical data were stored in a secure database at the Neuroscience Group of
248 Antioquia in Medellín, Colombia.

249

250 Sample collection

251 Brain samples were collected post-mortem and embedded in paraffin after fixation in
252 formalin. A neuropathological study was performed, in accordance with the NIA-A
253 guidelines[3]. Sections of 4 µm thick were stained with haematoxylin and eosin (H&E)
254 further processed for immunohistochemical (IHC) staining for amyloid beta (Aβ, 1:100;
255 BAM-10, Mob410; DBS Emergo Europe, The Hague, The Netherlands),
256 hyperphosphorylated Tau Ser 202 and Thr 205 (tau, 1:1500; AT8, MN1020;

257 ThermoFisher Scientific, Dreieich, Germany). Automatic immunostaining was
258 performed with a Ventana Benchmark XT system (Roche AG, Basel, Switzerland)
259 according to manufacturer instructions. Briefly, after dewaxing and inactivation of
260 endogenous peroxidases (PBS/3% hydrogen peroxide), antibody specific antigen
261 retrieval was performed, sections were blocked and afterwards incubated with the
262 primary antibody. For detection of specific binding, the Ultra View Universal 3,3´-
263 Diaminobenzidine (DAB) Detection Kit (Ventana, Roche) was used which contains
264 secondary antibodies, DAB stain and counter staining reagent. All slides were evaluated
265 by properly trained personnel. The olfactory bulbs and tracts were cut sagittally at 7 μm
266 thickness, placed longitudinally on slides and were embedded in paraffin.
267
268 Multispectral immunohistochemistry of the olfactory bulb and olfactory tract
269 Through our collaboration with the Human Immune Monitoring Shared Resource
270 (HIMSR) at the University of Colorado School of Medicine we performed multispectral
271 imaging using the Akoya Vectra Polaris instrument. This instrumentation allows for
272 phenotyping, quantification, and spatial relationship analysis of tissue infiltrate in
273 formalin-fixed paraffin-imbedded biopsy sections. Formalin-fixed paraffin-embedded
274 tissue sections were stained consecutively with specific primary antibodies according to
275 standard protocols provided by Akoya and performed routinely by the HIMSR. Briefly,
276 the slides were deparaffinized, heat treated in antigen retrieval buffer, blocked, and
277 incubated with primary antibodies against Aβ, Iba1, GFAP, Cleaved Caspase 3, p-Tau,
278 DCX, CD68, and PLP (Supplementary Table 2), followed by horseradish peroxidase
279 (HRP)-conjugated secondary antibody polymer, and HRP-reactive OPAL fluorescent
280 reagents that use TSA chemistry to deposit dyes on the tissue immediately surrounding

281 each HRP molecule. To prevent further deposition of fluorescent dyes in subsequent
282 staining steps, the slides were stripped in between each stain with heat treatment in
283 antigen retrieval buffer. Slides were finally counterstained with DAPI. Whole slide scans
284 were collected using the 10x objective and multispectral images were collected using the
285 20x objective with a 0.5 micron resolution. The 9-color images were analyzed with inForm
286 software V2.5 to unmix adjacent fluorochromes, subtract autofluorescence, segment the
287 tissue, compare the frequency and location of cells, segment cellular membrane,
288 cytoplasm, and nuclear regions, score each cellular compartment, and phenotype
289 infiltrating immune cells according to morphology and cell marker expression.
290
291 We used custom scripts in Fiji to quantify Aβ, Iba1, CD68 and PLP on the 20x objective
292 images. ROIs for high and low myelinated areas were manually determined using PLP
293 stain by two researchers. To quantify Aβ, Iba1 and CD68-positive areas, we defined the
294 positive area as one that exceeds n SDs of the mean image intensity, with $n = 2$ for Aβ and
295 Iba1 and $n = 4$ for CD68. The positive surface was expressed as a percentage of the ROI
296 surface per individual. Masks for each stain were created from the thresholded images,
297 and mask combinations were used to determine the double and triple-positive areas.
298
299 <u>FFPE TempO-Seq</u>
300 For whole human transcriptome analysis, FFPE slides from OB or OT were assayed using
301 TempO-Seq–targeted RNA sequencing plates, reagents, protocols, and software
302 (BioSpyder
303 Technologies). TempO-Seq exclusively detects human transcripts; viral transcripts were
304 not assayed. Visually identified H&E stained OB and OT tissue sections were scraped (~5-

305 10 mm^2), and placed into PCR tubes containing 1X lysis buffer. Using a thermocycler,
306 samples were lysed, coded adjacent primer pairs for each specific human transcript were
307 annealed to sample RNA, and primer pairs for each transcript ligated and then amplified
308 per manufacturer's instructions[4]. If a transcript is present, the adjacent 25-nucleotide
309 primer pairs anneal to their specific target, ligate together, and produce a 50-nucleotide
310 transcript-specific, coded amplicon.
311 Amplified PCR products were pooled into a single library, concentrated using a PCR
312 cleanup kit (Macherey-Nagel, Düren, Germany), and run on the Illumina NextSeq 500
313 sequencing platform (Illumina Inc., San Diego, CA). Mapped reads were generated by
314 TempO-SeqR for the alignment of demultiplexed FASTQ files from the sequencer to the
315 ligated detector oligomer gene sequences using Bowtie, allowing for up to 2 mismatches
316 in the 50-nucleotide target sequence[4]. Counts were assessed using SARTools[5]. Within this
317 R package, edgeR is used for normalization and quality control of count data[6]. Differential
318 expression between groups was assessed by the TempO-SeqR software, which used the
319 DESeq2 method for differential analysis of count data[7]. A significantly differentially
320 expressed gene is defined as having an adjusted p value < 0.05 with no fold-change
321 threshold.
322
323 Pathway enrichment analysis was performed using gene sets and pathways defined in the
324 Ingenuity Pathway Analysis software (Qiagen, Germantown, MD) and the ClusterProfiler
325 package[8,9] in R with default parameters. ClusterProfiler supports enrichment analysis of
326 Gene Ontology and Kyoto Encyclopedia of Genes and Genomes databases with Gene Set
327 Enrichment Analysis (GSEA) to identify biological themes of a collection of genes. These
328 functional enrichment analyses use computational approaches to identify groups of

329 experimentally observed human genes that are overrepresented or depleted in a curated
330 disease or biological function-specific gene set. Additional figures were created using
331 Prism 9 (GraphPad Software, San Diego, CA).
332
333 nanoString proteomics
334 We used nanoString proteomics for 88 proteins (Supplementary Table 3) with four
335 fluorescent markers to discriminate tissue regions (Supplementary Table 4) using
336 methods detailed by Merritt and co-workers[10]. Briefly, all assays were performed on 5-µm
337 FFPE sections mounted onto charged slides. Deparaffinization and rehydration of tissue
338 was performed by incubating slides in three washes of CitriSolv (Decon Labs, 1601) for 5
339 min each, two washes of 100% ethanol for 10 min each, two washes of 95% ethanol for 10
340 min each and two washes of distilled water for 5 min each. For antigen retrieval, slides
341 were then placed in a plastic Coplin jar containing 1× Citrate Buffer pH 6.0 (Sigma,
342 C9999) and covered with a lid. The Coplin jar was placed into a pressure cooker (BioSB,
343 BSB7008) that was run at high pressure and temperature for 15 min. The Coplin jar was
344 removed from the pressure cooker and cooled at room temperature for 25 min. Slides
345 were washed with five changes of 1× TBS-T (Cell Signaling Technology, 9997) for 2 min
346 each. Excess TBS-T was removed from the slide, and a hydrophobic barrier was drawn
347 around each tissue section with a hydrophobic pen (Vector Laboratories, H-4000). Slides
348 were then incubated with blocking buffer (1× TBS-T, 5% goat serum (Sigma-Aldrich,
349 G9023-5ML), 0.1 mg ml–1 salmon sperm DNA (Sigma-Aldrich, D7656) and 10 mg ml–1
350 dextran sulfate (Sigma-Aldrich, 67578-5G) for 1 h. Slides were washed with three changes
351 of 1× TBS-T for 2 min

352 each. Primary antibodies (Supplementary tables 3 and 4) were diluted in Buffer W
353 (GeoMx Protein Slide Prep Kit Item 121300312). Tissue sections were then covered with
354 diluted primary antibody solution (see above for morphology marker information). Slides
355 were incubated at 4 °C in a humidity chamber overnight. Primary antibody was aspirated
356 from slides, and slides were washed with three changes of 1× TBS-T for 10 min each.
357 Antibodies were postfixed with 4% paraformaldehyde for 30 min at room temperature
358 and then wasted twice in TBS-T. DNA was counterstained with 500 nM SYTO13 (Thermo
359 Fisher, S7575) in 1× TBS-T or TBS for 15 min. Excess DNA counterstain was removed with
360 five changes of TBS-T, and slides were the processed on the GeoMx instrument as
361 described in Merritt et al[10].
362
363 Statistical analysis
364 Matlab or Excel were used to perform t tests or ANOVAs, followed by post-hoc Fisher's
365 least significant difference procedure.
366
367

368 1. Quiroz, Y.T., *et al.* Association Between Amyloid and Tau Accumulation in Young Adults
369 With Autosomal Dominant Alzheimer Disease. *JAMA Neurology* **75**, 548-556 (2018).
370 2. Acosta-Baena, N., *et al.* Pre-dementia clinical stages in presenilin 1 E280A familial early-
371 onset Alzheimer's disease: a retrospective cohort study. *The Lancet Neurology* **10**, 213-220
372 (2011).
373 3. Montine, T.J., *et al.* National Institute on Aging–Alzheimer's Association guidelines for
374 the neuropathologic assessment of Alzheimer's disease: a practical approach. *Acta*
375 *Neuropathologica* **123**, 1-11 (2012).

376 4. Trejo, C.L., *et al.* Extraction-free whole transcriptome gene expression analysis of FFPE
377 sections and histology-directed subareas of tissue. *PLoS One* **14**, e0212031 (2019).
378 5. Varet, H., Brillet-Gueguen, L., Coppee, J.Y. & Dillies, M.A. SARTools: A DESeq2- and
379 EdgeR-Based R Pipeline for Comprehensive Differential Analysis of RNA-Seq Data.
380 *PLoS One* **11**, e0157022 (2016).
381 6. Robinson, M.D., McCarthy, D.J. & Smyth, G.K. edgeR: a Bioconductor package for
382 differential expression analysis of digital gene expression data. *Bioinformatics* **26**, 139-140
383 (2010).
384 7. Love, M.I., Huber, W. & Anders, S. Moderated estimation of fold change and dispersion
385 for RNA-seq data with DESeq2. *Genome Biol* **15**, 550 (2014).
386 8. Yu, G., Wang, L.-G., Han, Y. & He, Q.-Y. clusterProfiler: an R Package for Comparing
387 Biological Themes Among Gene Clusters. *OMICS: A Journal of Integrative Biology* **16**,
388 284-287 (2012).
389 9. Yu, G., Wang, L.-G., Yan, G.-R. & He, Q.-Y. DOSE: an R/Bioconductor package for
390 disease ontology semantic and enrichment analysis. *Bioinformatics* **31**, 608-609 (2015).
391 10. Merritt, C.R., *et al.* Multiplex digital spatial profiling of proteins and RNA in fixed tissue.
392 *Nature Biotechnology* **38**, 586-599 (2020).
393
394

395 **Supplementary Materials**

396

397 **Signatures for Viral Infection and Inflammation in the Proximal Olfactory**

398 **System in Familial Alzheimer's Disease**

399

400 Andrew N. Bubak[1,‡], Laetitia Merle[2,3,‡], Christy S. Niemeyer[1], B. Dnate' Baxter[2,3],

401 Arianna Gentile Polese[2,3], Vijay Ramakrishnan[4], Johana Gomez[5], Lucia Madrigal[5],

402 Andres Villegas-Lanau[5], Francisco Lopera[5], Wendy Macklin[1,2], Seth Frietze[6], Maria A.

403 Nagel[5,#], and Diego Restrepo[1,2, #,*]

404

405 [1]Department of Neurology, University of Colorado Anschutz Medical Campus, Aurora,

406 CO 80045, USA

407 [2]Neuroscience Graduate Program, University of Colorado Anschutz Medical Campus,

408 Aurora, CO 80045, USA

409 [3]Department of Cell and Developmental Biology, University of Colorado Anschutz

410 Medical Campus, Aurora, CO 80045, USA

411 [4]Department of Otolaryngology-Head and Neck Surgery, Indiana University School of

412 Medicine, Indianapolis, IN 46202, USA

413 [5]Neuroscience Research Group, University of Antioquia, Medellín, Colombia

414 [6]Department of Medical Laboratory Sciences, University of Vermont, Burlington, VT

415 [‡]Co-first authors

416 [#]Senior authors

417

418

419 **Supplementary Note 1. Annotations regarding the function of proteins in**
420 **groups A and B of the nanoString (Fig. 2Dii)**
421
422 **nanoString group A proteins: high expression in FAD high myelination OT**
423 **(Fig. 2B)**
424
425 The majority of these proteins are involved in demyelination or are axonal proteins.
426
427 **Neurofilament light.** Neurofilament light chain (NfL) is a neuronal cytoplasmic
428 protein highly expressed in large calibre myelinated axons [1].
429
430 **Fibronectin (FN1).** In toxin-induced lesions undergoing efficient remyelination,
431 fibronectin expression was transiently increased within demyelinated areas and
432 declined as remyelination proceeded[2].
433
434 **INPP4B.** EAE31 is a locus controlling latency of motor evoked potentials (MEPs) and
435 clinical onset of experimental autoimmune encephalomyelitis. By combining congenic
436 mapping, *in silico* haplotype analyses, and comparative genomics Lemcke and co-
437 workers identified inositol polyphosphate-4-phosphatase, type II (*Inpp4b*) as the
438 quantitative trait gene for EAE31[3].
439
440 **CD25 (IL2RA).** Depletion of $CD4^+CD25^+$ cells *in vivo* facilitated the expansion of PLP
441 reactive cells with production of T helper 1 cytokines in EAE-resistant B10.S mice.
442 Furthermore, anti-CD25 Ab treatment before immunization resulted in EAE induction

443 in these otherwise resistant mice. These data indicate an important role for autoantigen-
444 specific $CD4^{+}CD25^{+}$ cells in genetic resistance to autoimmunity[4].
445
446 **Ubiquitin.** The vast majority of cellular proteins are degraded by the 26S proteasome
447 after their ubiquitination. Belogurov et al. [5] report that the major component of the
448 myelin multilayered membrane sheath, myelin basic protein (MBP), is hydrolyzed by
449 the 26S proteasome in a ubiquitin-independent manner both *in vitro* and in
450 mammalian cells[5].
451
452 **PD.L2.** Programed death ligand 2. PD-L2 is up-regulated in inflamed endothelial cells,
453 with an intention to inhibit T-cell transmigration through the blood brain barrier{Zhao,
454 2014 #4650}.
455
456 **ICOS.** The inducible costimulatory molecule (ICOS) is expressed on activated T cells
457 and participates in a variety of important immunoregulatory functions. After the
458 induction of experimental allergic encephalomyelitis in SJL mice with proteolipid
459 protein (PLP), brain ICOS mRNA and protein were up-regulated on infiltrating CD3+ T
460 cells before disease onset.[6]
461
462 **CD80.** CD4+ T Cell Expressed CD80 Regulates Central Nervous System Effector
463 Function and Survival during Experimental Autoimmune Encephalomyelitis[7].
464

465 **PD.1 and PD.L1.** The review by Cencioni et al describes the roles of the PD-1/ PDL-1
466 pathway in cancer and autoimmune diseases, especially in multiple sclerosis, and how
467 manipulating PD-1 can be a therapeutic approach in multiple sclerosis[8].
468
469 **Phospho-PRAS40..T246. PRAS40** (Proline-rich AKT1 substrate 1), also known
470 as Akt1S1 and p39, is a 40-42 kDa cytoplasmic phosphoprotein that lacks generally
471 recognized structural motifs. It is widely expressed and is considered to be key regulator
472 of mTORC1 (mTOR plus Raptor and G beta L), a complex through which Akt signals
473 into the cell. Through phosphorylation, mTORC1 activity is upregulated by PRAS40[9].
474
475 **Phospho-AKT1..S473.** Involved in the dual function of the PI3K-Akt-mTORC1 axis in
476 myelination of the peripheral nervous system[10].
477
478 **Phsopho-GSK3B.S9.** MAI-dependent phosphorylation and inactivation of GSK3beta
479 regulate phosphorylation of CRMP4, a cytosolic regulator of myelin inhibition, and its
480 ability to complex with RhoA[11].
481
482 **Vimentin.** Increase in tissue stiffness elicited by chronic demyelination of the corpus
483 callosum is accompanied by astrogliosis, as shown by elevated GFAP and vimentin
484 staining[12].
485
486 **CD68.** This is a marker for macrophages. Myelin loss along with axonal destruction, the
487 pathological hallmark of metachromatic leukodystrophy is thought to be caused by
488 critical sulphatide levels in oligodendrocytes and Schwann cells. Immunolabelling with

489 MBP and CD68 showed a gradient of demyelination from near-intact U-fibres to
490 myelin-depleted white matter with diffuse macrophage infiltration.[13].
491
492 **APP.** Data by Truong et al. identified APP and APLP2 as modulators of normal
493 myelination and demyelination/remyelination conditions. Deletion of APP and APLP2
494 identifies novel interplays between the BACE1 substrates in the regulation of
495 myelination[14].
496
497 **Myelin basic protein.** MBP is a protein found in the myelin sheath.
498
499 **CD45RO.** Dual expression of CD45RA and CD45RO isoforms on myelin basic protein-
500 specific CD4+ T-cell lines in multiple sclerosis[15]
501
502 **nanoString group B proteins: high expression in FAD low myelination OT**
503
504 These proteins are AD markers.
505
506 **IDE.** Insulin-degrading-enzyme plays a crucial role in the clearance of amyloid-β and
507 has been proposed as a therapeutical target for Alzheimer's disease[16].
508
509 **ADAM10.** ADAM10 is involved in the proteolytic processing of the amyloid precursor
510 protein[17]. ADAM10 also cleaves the ectodomain of the triggering receptor expressed on
511 myeloid cells 2 (TREM2), to produce soluble TREM2 (sTREM2), which has been
512 proposed as a CSF and sera biomarker of neurodegeneration[18].

513

514

515 **NRGN.** Neurogranin concentration in cerebrospinal fluid (CSF) is proposed as marker
516 for synaptic dysfunction in age-related neurodegeneration[19], and has been shown to be
517 specifically increased in patients with Alzheimer's disease[20].

518

519 **Synaptophysin.** In the TMEV model, only a few large- to medium-sized
520 synaptophysin/APP-positive bulbs were found in demyelinated areas. In MS patient
521 tissue samples, the bulbs appeared exclusively at the inflammatory edges of lesions. In
522 conclusion, our data suggest that synaptophysin as a reliable marker of axonal damage
523 in the CNS in inflammatory/demyelinating conditions[21].

524

525 **PLCG1.** Phospholipase C, gamma 1 gene mutations and abnormal splicing of PLCγ1
526 gene has been identified in AD using both high-throughput screening data and a deep
527 learning-based prediction[22].

528

529 **S6.** Ribosomal protein S6

530

531 **Phospho Tuberin T1462.** The control of translation is disturbed in Alzheimer's
532 disease (AD). Morel et al.[23] analyzed the crosslink between the up regulation of double-
533 stranded RNA-dependent-protein kinase (PKR) and the down regulation of mammalian
534 target of rapamycin (mTOR) signaling pathways via p53, the protein Regulated in the
535 Development and DNA damage response 1 (Redd1) and the tuberous sclerosis complex
536 (TSC2) factors in two beta-amyloid peptide (Abeta) neurotoxicity models. In SH-SY5Y

537 cells, Abeta42 induced an increase of P(T451)-PKR and of the ratio p66/(p66+p53) in
538 nuclei and a physical interaction between these proteins. Redd1 gene levels increased
539 and P(T1462)-TSC2 decreased. These disturbances were earlier in rat primary neurons
540 with nuclear co-localization of Redd1 and PKR. The PKR gene silencing in SH-SY5Y cells
541 prevented these alterations. p53, Redd1 and TSC2 could represent the molecular links
542 between PKR and mTOR in Abeta neurotoxicity. PKR could be a critical target in a
543 therapeutic program of AD.
544
545 **Tau, Phospho.Tau..S199.** Phosphorylated tau.
546
547
548
549
550
551

552 **Supplementary Table 1. Patient information**

Subject ID	Group	Age	Sex	Cause of Death	OT surface analyzed in Vectra (mm2)	Temp-O-SEQ OT	Temp-O-SEQ OB	Nanostring OT	Nanostring OB
337	Control	84	M	Bacterial pneumonia	5.1	X	X	X	X
351	Control	62	M	Heart failure	7.0		X		
354	Control	65	M	Decompensated chronic obstructive pulmonary disease	3.3		X		
360	Control	72	M	Acute myocardial infarction	2.1	X			
364	Control	73	M	Gastric cancer	3.9	X			
380	Control	56	F	Colon cancer	4.1	X	X	X	X
359	FAD (E280A)	56	F	Bacterial pneumonia	3.6	X	X	X	X
346	FAD (E280A)	53	M	Aspiration pneumonia	5.2	X	X		
355	FAD (Late Onset)	86	F	Acute renal failure	3.0	X	X		
335	FAD (E280A)	59	M	Bacterial pneumonia	2.7	X	X		
358	FAD (E280A)	59	F	Aspiration pneumonia	1.1	X	X	X	X
382	FAD (E280A)	57	F	Metabolic imbalance	3.8	X	X		

553

554

555

556 **Supplementary Table 2. Antibody information for multispectral immunohistochemistry**

Target	Concentration	Antigen retrieval conditions	Vendor	Catalogue number	Host Species
Ab	1:500	EDTA ER2 pH9	Biolegend	803001	Mouse
Iba1	1:10,000	EDTA ER2 pH9	Wako	019-19741	Rabbit
GFAP	1:500	EDTA ER2 pH9	Dako/Agilent	Z033429-2	Rabbit
Cleaved Caspase 3	1:100	EDTA ER2 pH9	Cell Signaling	9664L	Rabbit
p-Tau	1:200	Citrate ER1 pH6	Invitrogen	MN1020	Mouse
DCX	1:5,000	Citrate ER1 pH6	Abcam	ab18723	Rabbit
CD68	1:500	Citrate ER1 pH6	Dako/Agilent	M0814	Mouse
PLP	1:400	Citrate AR buffer + TritonX100 pH6	PLP antibody source was[24]		Rat

557
558 Antigen retrieval was performed on a fully automated immunostainer using either ER1 (citrate with a pH
559 range of 5.9-6.1) or ER2 (EDTA with a pH range of 8.9-9.1) buffers, except for PLP which was manually
560 processed in the microwave with citrate AR buffer and TritonX100 (pH6).

561 **Supplementary Table 3. Excel worksheet with TempO-Seq raw counts and p-values for all**
562 **genes for the olfactory tract (control vs. FAD)**

563

564 **Supplementary Table 4. Excel worksheet with TempO-Seq raw counts and p-values for all**
565 **genes for the olfactory bulb (control vs. FAD)**

566

567 **Supplementary Table 5. Excel worksheet with genes included in specific pathways by**
568 **Insight analysis.**

569 **Supplementary Table 6. Antibodies used for nanoString**

570

Item name	Item Number
GeoMx Human Protein Core for NGS	121300129
GeoMx Immune Cell Typing Assay	121300130
GeoMx Immune Activation Status Assay	121300132
GeoMx Myeloid Assay	121300137
GeoMx PI3K/AKT Signaling Assay	121300136
GeoMx Neural Cell Typing Assay	121300138
GeoMx Alzheimer's Pathology Assay	121300139
GeoMx Glial Cell Subtyping Assay	121300143

571

572

573 **Supplementary Table 7. Antibody information for immunofluorescence for nanoString**

Antibody ID	Name	company	clone #	Catalog #	concentration used
syto13	syto13	NanoString		121300306	25
MF-304	Beta amyloid	Novus	MOAB-2	NBP2-13075AF532	1:100
MF-618	MBP	Novus	2H9	NBP2-22121AF594	1:100
MF-643	Iba1	millipore	20A12.1	MABN92-AF647	1:100

574

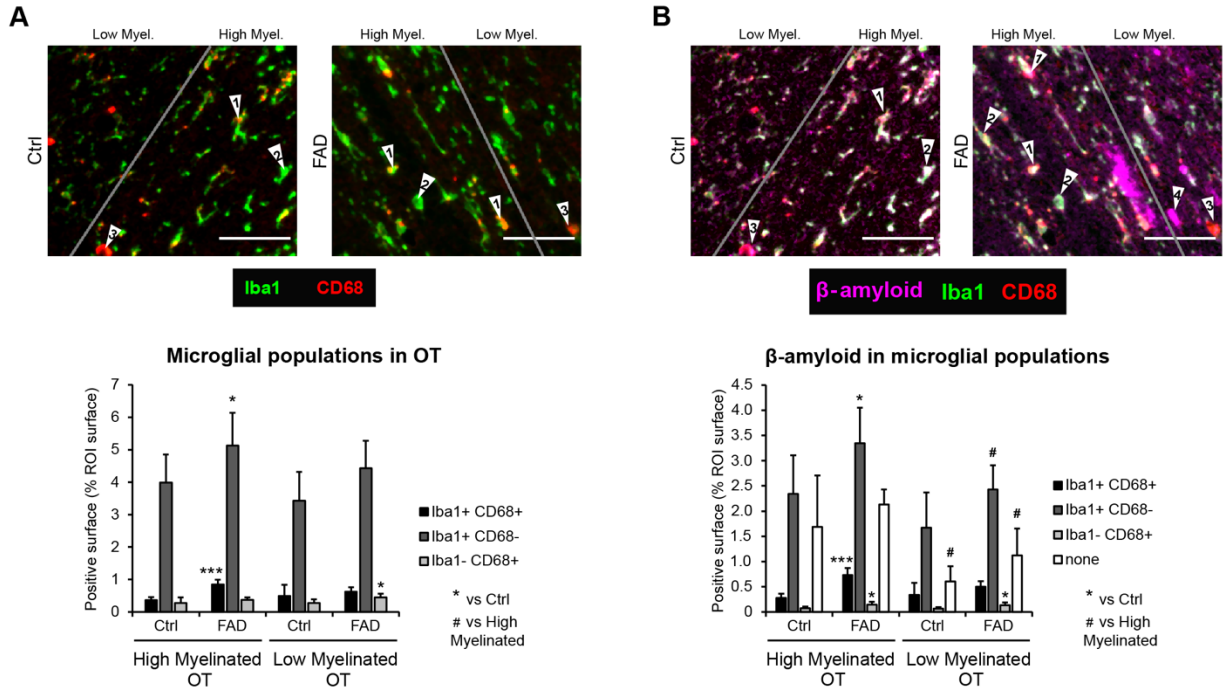

575

576 **Supplementary Figure 1. Microglial populations in the OT. A.** Quantification of the 3 different
577 microglial populations: Iba1+CD68+ (arrows "1"), Iba1+CD68- (arrows "2"), Iba1-CD68+
578 (arrows "3"). An ANOVA yields a significant difference for the genotype for Iba1+CD68+
579 (F=14.1, 1 d.f., p<0.01), Iba1+CD68- (F=8, 1 d.f., p<0.05) and Iba1-CD68+ (F=6.65, 1 d.f.,
580 p<0.05). FAD patients exhibit an increase in Iba1+CD68+ surface and Iba1+CD68- surface in the
581 high myelinated OT, and an increase in Iba1-CD68+ surface low myelinated OT, compared to
582 Ctrl. **B.** An ANOVA yields a significant difference for the genotype for Aβ surface that is
583 overlapping with Iba1+CD68+ cells (F=24.14, 1 d.f., p<0.001), Iba1+CD68- cells (F=9.93, 1 d.f.,
584 p<0.01) and Iba1-CD68+ cells (F=12.28, 1 d.f., p<0.01). An ANOVA yields a significant
585 difference between high and low myelination areas for Aβ surface that is overlapping with
586 Iba1+CD68- cells (F=8, 1 d.f., p<0.05) and Aβ free from microglial coverage (F=15.93, 1 d.f.,
587 p<0.001). Aβ surface that is overlapping with all three microglial populations is increased in the
588 high myeline OT of FAD patients compared to Ctrl. Aβ surface that is overlapping with Iba1-

589 CD68+ cells is increased in the low myeline OT. Aβ free from microglial coverage (arrows “4”)
590 is decreased in the low myeline OT compared to the high myeline OT in both Ctrl and FAD. Scale
591 bar: 50 µm.
592

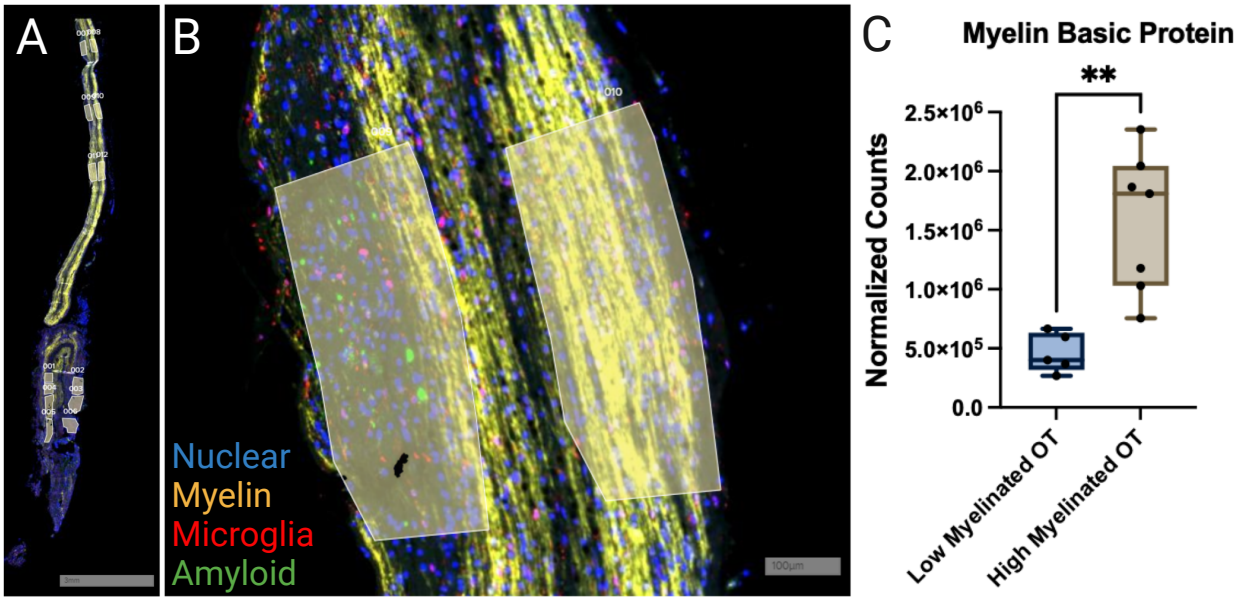

Supplementary Figure 2. Quantification of expression of myelin basic protein in the high and low myelinated regions of the OT of FAD subjects using nanoString spatial profiling. **A.** A representative horizontal tissue section (FAD 359) of the OB/OT showing regions used for protein quantification. The sections are immunolabeled for myelin basic protein, Iba1, Aβ and nuclear staining (styo13). **B.** Closeup of OT areas with high and low myelination. **C.** Normalized counts for myelin basic protein in the low and high myelination areas. The difference is statistically significant ($p<0.05$, pairwise t-test).

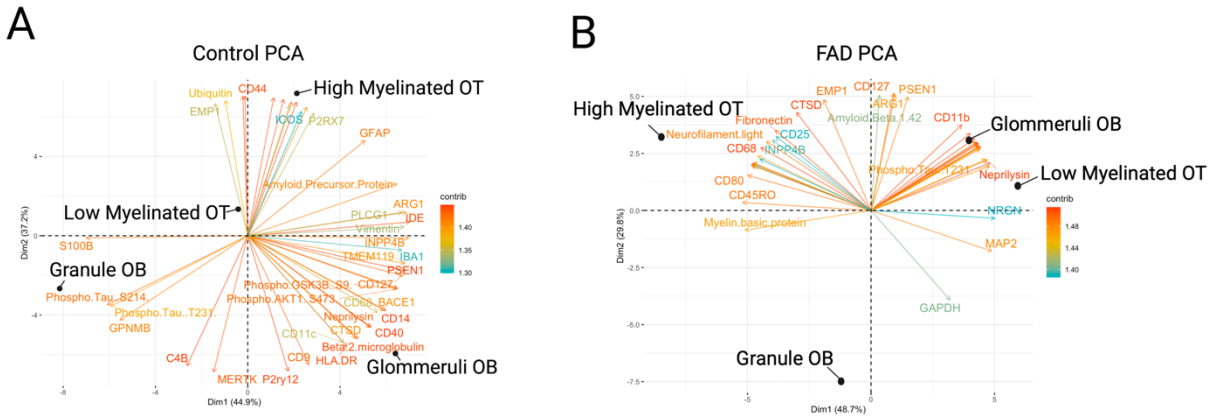

Supplementary Figure 3. Principal component analysis of the proteomic data for the control and FAD datasets. A principal component analysis of nanoString protein expression shows increased distance between high and low myelinated OT in the FAD tissue. A. Control. B. FAD.

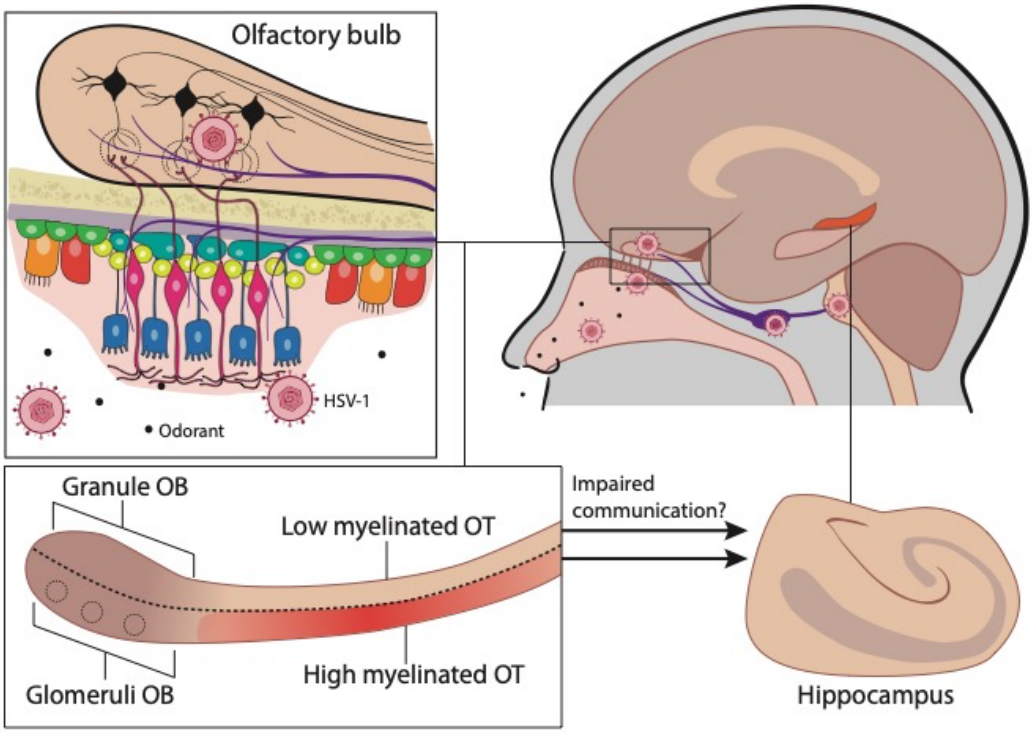

608

609 **Supplementary Figure 4. Diagram illustrating the finding of viral infection of the olfactory**

610 **bulb and altered response to demyelination in the olfactory tract of FAD patients.**

611 1. Gaetani, L., *et al.* Neurofilament light chain as a biomarker in neurological disorders.
612 *Journal of Neurology, Neurosurgery & Psychiatry* **90**, 870 (2019).
613 2. Stoffels, J.M.J., *et al.* Fibronectin aggregation in multiple sclerosis lesions impairs
614 remyelination. *Brain* **136**, 116-131 (2013).
615 3. Lemcke, S., *et al.* Nerve Conduction Velocity Is Regulated by the Inositol Polyphosphate-
616 4-Phosphatase II Gene. *The American Journal of Pathology* **184**, 2420-2429 (2014).
617 4. Reddy, J., *et al.* Myelin proteolipid protein-specific
618 CD4⁺CD25⁺ regulatory cells mediate
619 genetic resistance to experimental autoimmune encephalomyelitis. *Proceedings of the*
620 *National Academy of Sciences of the United States of America* **101**, 15434 (2004).
621 5. Belogurov, A., Jr., *et al.* Multiple Sclerosis Autoantigen Myelin Basic Protein Escapes
622 Control by Ubiquitination during Proteasomal Degradation *. *Journal of Biological*
623 *Chemistry* **289**, 17758-17766 (2014).
624 6. Rottman, J.B., *et al.* The costimulatory molecule ICOS plays an important role in the
625 immunopathogenesis of EAE. *Nature Immunology* **2**, 605-611 (2001).
626 7. Podojil, J.R., Kohm, A.P. & Miller, S.D. CD4⁺ T Cell Expressed
627 CD80 Regulates Central Nervous System Effector Function and Survival during
628 Experimental Autoimmune Encephalomyelitis. *The Journal of Immunology* **177**, 2948
629 (2006).
630 8. Cencioni, M.T. The immune regulation of PD-1/PDL-1 axis, a potential biomarker in
631 multiple sclerosis. *Neuroimmunology and Neuroinflammation* **7**, 277-290 (2020).
632 9. Bercury, K.K., *et al.* Conditional ablation of raptor or rictor has differential impact on
633 oligodendrocyte differentiation and CNS myelination. *J Neurosci* **34**, 4466-4480 (2014).

634 10. Figlia, G., Norrmén, C., Pereira, J.A., Gerber, D. & Suter, U. Dual function of the PI3K-
635 Akt-mTORC1 axis in myelination of the peripheral nervous system. *eLife* **6**, e29241
636 (2017).
637 11. Alabed, Y.Z., Pool, M., Ong Tone, S., Sutherland, C. & Fournier, A.E. GSK3β Regulates
638 Myelin-Dependent Axon Outgrowth Inhibition through CRMP4. *The Journal of*
639 *Neuroscience* **30**, 5635 (2010).
640 12. Urbanski, M.M., Brendel, M.B. & Melendez-Vasquez, C.V. Acute and chronic
641 demyelinated CNS lesions exhibit opposite elastic properties. *Scientific Reports* **9**, 999
642 (2019).
643 13. Ponath, G.*, et al.* Myelin phagocytosis by astrocytes after myelin damage promotes lesion
644 pathology. *Brain* **140**, 399-413 (2017).
645 14. Truong, P.H.*, et al.* Amyloid precursor protein and amyloid precursor-like protein 2 have
646 distinct roles in modulating myelination, demyelination, and remyelination of axons. *Glia*
647 **67**, 525-538 (2019).
648 15. Qin, Y., van den Noort, S., Kurt, J. & Gupta, S. Dual expression of CD45RA and CD45RO
649 isoforms on myelin basic protein-specific CD4+ T-cell lines in multiple sclerosis. *Journal*
650 *of Clinical Immunology* **13**, 152-161 (1993).
651 16. Kurochkin, I.V., Guarnera, E. & Berezovsky, I.N. Insulin-Degrading Enzyme in the Fight
652 against Alzheimer's Disease. *Trends in Pharmacological Sciences* **39**, 49-58 (2018).
653 17. Haass, C., Kaether, C., Thinakaran, G. & Sisodia, S. Trafficking and proteolytic processing
654 of APP. *Cold Spring Harb Perspect Med* **2**, a006270 (2012).
655 18. Yang, J.*, et al.* TREM2 ectodomain and its soluble form in Alzheimer's disease. *Journal*
656 *of Neuroinflammation* **17**, 204 (2020).

657 19. Casaletto, K.B., *et al.* Neurogranin, a synaptic protein, is associated with memory
658 independent of Alzheimer biomarkers. *Neurology* **89**, 1782 (2017).
659 20. Willemse, E.A.J., *et al.* Neurogranin as Cerebrospinal Fluid Biomarker for Alzheimer
660 Disease: An Assay Comparison Study. *Clinical Chemistry* **64**, 927-937 (2018).
661 21. Gudi, V., *et al.* Synaptophysin Is a Reliable Marker for Axonal Damage. *Journal of*
662 *Neuropathology & Experimental Neurology* **76**, 109-125 (2017).
663 22. Kim, S.-H., *et al.* Prediction of Alzheimer's disease-specific phospholipase c gamma-1
664 SNV by deep learning-based approach for high-throughput screening. *Proceedings of the*
665 *National Academy of Sciences* **118**, e2011250118 (2021).
666 23. Morel, M., *et al.* Evidence of molecular links between PKR and mTOR signalling pathways
667 in Aβ neurotoxicity: Role of p53, Redd1 and TSC2. *Neurobiology of Disease* **36**, 151-161
668 (2009).
669 24. Yamamura, T., Konola, J.T., Wekerle, H. & Lees, M.B. Monoclonal Antibodies Against
670 Myelin Proteolipid Protein: Identification and Characterization of Two Major
671 Determinants. *Journal of Neurochemistry* **57**, 1671-1680 (1991).
672